MAXIMUM LIFT OF WINGS WITH TRAILING-EDGE FLAPS AT LOW SPEEDS

1. NOTATION AND UNITS

		SI	British
A	aspect ratio, $2s/\bar{c}$		
C_L	lift coefficient; (lift per unit span)/qc for aerofoil, (lift)/qS for wing		
C_{LL}	wing local lift coefficient; (lift per unit span)/qc		
C_{LLp}	peak (*i.e.* maximum) value of C_{LL}		
C_{Lmax}	wing maximum lift coefficient		
C_{LmaxB}	wing maximum lift coefficient with high-lift devices undeployed (*i.e.* “basic” wing)		
C_{Lm}	aerofoil section maximum lift coefficient		
ΔC_{Lmaxt}	increment in wing maximum lift coefficent due to deployment of trailing-edge flaps		
ΔC_{Lmt}	increment in aerofoil section maximum lift coefficient due to deployment of trailing-edge flap, based on c		
$\Delta C'_{Lmt}$	increment in aerofoil section maximum lift coefficient due to deployment of trailing-edge flap, based on c'		
c	wing local chord, see Sketch 1.1; basic aerofoil section chord	m	ft
c'	wing extended local chord	m	ft
c_p	wing chord at spanwise location of peak loading due to incidence, see Sketch 1.1	m	ft
c_r	wing root (centre-line) chord	m	ft
c_t	chord of trailing-edge flap	m	ft
$\bar{c}$	wing geometric mean chord	m	ft
$\bar{\bar{c}}$	wing aerodynamic mean chord	m	ft
F_R	factor for effect of Reynolds number on ΔC_{Lmaxt}, see Equation (6.6)		
K_f	correlation factor dependent on flap type, see Section 6.2		

Issued August 1991
With Amendment A, August 1995

$K_{\Lambda t}$	correlation factor for wing sweep, see Equation (6.7)		
M	free-stream Mach number		
q	free-stream kinetic pressure	N/m^2	lbf/ft^2
R_c	Reynolds number based on free-stream conditions and c		
$R_{\bar{\bar{c}}}$	Reynolds number based on free-stream conditions and $\bar{\bar{c}}$		
S	wing planform area, $2s\bar{c}$	m^2	ft^2
s	wing semi-span	m	ft
t	maximum thickness of aerofoil	m	ft
z_{cm}	maximum height of camber line of basic aerofoil (see Item No. 94029)	m	ft
z_{lm}	lower-surface ordinate of basic aerofoil for which distance from chord line is maximum (see Item No. 94029)	m	ft
$z_{u1.25}$	upper-surface ordinate of basic aerofoil at 1.25% chord (see Item Nos 94029, 94030, 94031)	m	ft
β	compressibility parameter, $(1-M^2)^{½}$		
δ_t, δ°_t	deflection angle of trailing-edge flap, measured streamwise (see Item Nos 94028, 94029)	rad, deg	rad, deg
δ_{tj}, δ°_{tj}	deflection angle of element j of trailing-edge flap relative to datum of preceding element, measured streamwise (see Item Nos 94030, 94031)	rad, deg	rad, deg
ζ_p	leading-edge shape parameter for section normal to leading edge at $\eta = \eta_p, (z_{u1.25}/c)_p \sec\Lambda_0$		
η	spanwise distance from wing centre-line as fraction of semi-span		
η_i	value of η at inboard limit of flap		
η_o	value of η at outboard limit of flap		
η_p	value of η for μ_p		
$\bar{\eta}$	spanwise centre of pressure position for loading due to incidence (see Item No. 83040)		
κ	wing taper parameter in Item No. 83040; $\int_0^1 (c/\bar{c})\eta\,d\eta$, giving $(1+2\lambda)/[3(1+\lambda)]$ for straight-tapered wing		
Λ_h	flap hinge-line sweep angle (see Section 6.3)	deg	deg

Λ_0	wing leading-edge sweep angle, see Sketch 1.1	deg	deg
$\Lambda_{¼}$	wing quarter-chord sweep angle	deg	deg
$\Lambda_{½}$	wing mid-chord sweep angle	deg	deg
Λ_1	wing trailing-edge sweep angle, see Sketch 1.1	deg	deg
λ	wing taper ratio, (tip chord)/(root chord)		
μ	normalised local lift coefficient, C_{LL}/C_L		
μ_p	peak (*i.e.* maximum) value of μ		
ρ_l	aerofoil leading-edge radius	m	ft
Φ	part-span factor; lift coefficient increment due to part-span flaps extending symmetrically from wing centre-line divided by lift coefficient increment due to full-span flaps at same flap setting and wing angle of attack		
Φ_i	value of Φ corresponding to η_i, Figure 3a or 3b		
Φ_o	value of Φ corresponding to η_o, Figure 3a or 3b		
ϕ_t°	angle between basic aerofoil datum chord at trailing edge and upper surface, projected if necessary (see Item No. 94028)	deg	deg

Subscripts

p	denotes value for section at η_p
$(\ )_{expt}$	denotes experimental value
$(\ )_{pred}$	denotes predicted value

Superscript

$^\circ$	denotes angle in degrees

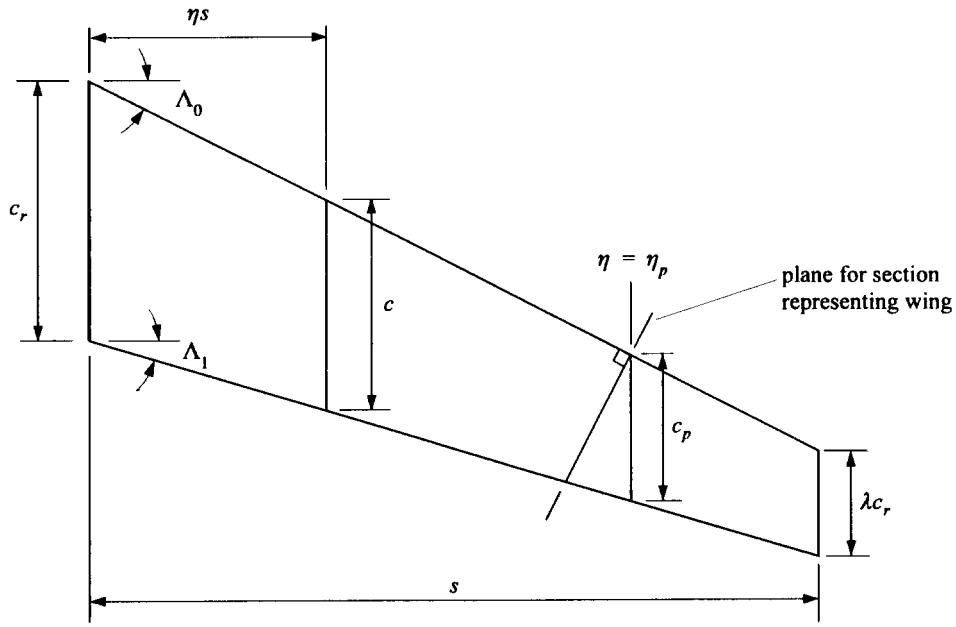

Sketch 1.1 Wing notation

2. INTRODUCTION

In this Item the increment in maximum lift coefficient due to the deployment of trailing-edge flaps on a wing is derived from the increment in maximum lift coefficient due to deployment of a trailing-edge flap on an aerofoil section representative of the wing. For wings with full-span high-lift devices the three-dimensional effects are similar to those for a plain wing (*i.e.* a wing with or without camber or twist but without deployment of manoeuvre or high-lift devices such as leading-edge or trailing-edge flaps); separation usually starts near the most highly loaded spanwise station and spreads rapidly with increasing incidence. For this reason the basic concepts with regard to the importance of the spanwise loading and the relevance of the most highly loaded section used in Item No. 89034 (Derivation 5) are maintained in this Item.

Item No. 84026 (Derivation 4) provides a method for the prediction of the maximum lift coefficient of aerofoils. Item Nos 94026 to 94031 (Derivations 6 to 11) provide methods for the prediction of the increment in the maximum lift coefficient of aerofoils due to the deployment of leading-edge or trailing-edge high-lift devices. Item No. 89034 provides a method for the prediction of the maximum lift coefficient of plain, cambered and twisted wings which utilises the aerofoil section data of Item No. 84026. This Item extends the scope of Item No. 89034 to provide the increment in maximum lift coefficient of wings due to the deployment of trailing-edge devices. The maximum lift coefficient of wings with trailing-edge high-lift devices deployed can therefore be obtained by the use of this Item in combination with Item No. 89034.

For subsonic speeds, the increment in maximum lift coefficient due to the deployment of trailing-edge flaps on a high aspect ratio wing is, to a first approximation, determined by the increment in the maximum lift coefficient due to the flaps on the aerofoil section. The main parameters which influence the increment in maximum lift coefficient due to flaps on an aerofoil section are the change in chord length due to trailing-edge flap deployment, aerofoil section geometry, the effective chord of the flap, the type of flap, Reynolds number and Mach number. For flaps on wings, additional parameters influence the maximum lift coefficient, in particular aspect ratio, taper ratio, sweep and spanwise extent of the flap. The estimation of the effects of leading-edge device deployment, without and with deployed trailing-edge flaps, is dealt with in Item No. 92031 (Reference 35).

3. REQUIRED DATA ITEMS

The ESDU Data Items that may be required in the use of this Item are:

Data Item No.	*Derivation No.*	*For Determination of*
76003	2	Various geometrical relationships for wings.
83040	3	Spanwise centre of pressure location.
84026	4	Aerofoil maximum lift coefficient for $M \approx 0$.
89034	5	Maximum lift coefficient of plain wings at subsonic speeds.
		Increment in aerofoil maximum lift coefficient due to deployment of:
94028	8	plain trailing-edge flaps,
94029	9	trailing-edge split flaps,
94030	10	single-slotted trailing-edge flaps,
94031	11	double-slotted and triple-slotted trailing-edge flaps.

4. SCOPE OF THE ITEM

The method of obtaining the maximum lift coefficient increment of the wing due to a trailing-edge flap, ΔC_{Lmaxt}, involves the evaluation of the increment, $\Delta C'_{Lmt}$, due to the deployment of the flap on the aerofoil section at the spanwise location of the peak loading due to incidence. The value of $\Delta C'_{Lmt}$, obtained from any of Item Nos 94028 to 94031, is then factored to allow for the effects of aspect ratio, taper and sweep and part-span effects. It has been found that similar factors apply for all types of trailing-edge flap. The method can therefore be used for all those trailing-edge flaps considered in Item Nos 94028 to 94031, which comprise plain, split, single-, double- and triple-slotted flaps. Although data used in the derivation of this Item did not include triple-slotted flaps it is believed that the method will be equally applicable.

The ranges of geometrical and flow parameters for the experimental data from which the correlation factors have been derived are given in Table 7.1.

5. EFFECTS OF MACH NUMBER AND REYNOLDS NUMBER

5.1 Mach Number Effects

High local Mach numbers will occur at low free-stream Mach number as a result of the deployment of high-lift devices. Mach number effects will occur at free-stream Mach numbers greater than about 0.2, depending on detailed section geometry. None of the data considered for this Item was for a Mach number greater than 0.25.

5.2 Reynolds Number Effects

Reynolds number effects for aerofoils are allowed for in the prediction of $\Delta C'_{Lmt}$ in Item Nos 94028 to 94031. For the data used in the derivation of this Item no additional effects of Reynolds number on ΔC_{Lmaxt} were found. However, it should be noted that in wind-tunnel tests with slotted flaps at very low Reynolds number ($R_{\bar{c}} < 0.6 \times 10^6$, say) the relatively thicker boundary layer reduces the effectiveness of the slot, thus reducing ΔC_{Lmaxt}. If estimates are required for single-slotted flaps at such low Reynolds numbers,

the use of plain flap data may yield a more representative result.

The effects of Reynolds number on C_{LmaxB}, the maximum lift coefficient of the basic wing with no high-lift devices deployed, are dealt with in Item No. 89034.

6. PREDICTION METHOD

6.1 Derivation of Method

Reports considered in the development of the method include work by Young, Roshko, McRae and Sanders (Derivations 24, 27, 28 and 29). The main effects of aspect ratio, taper ratio and the effects of sweep on the spanwise loading are allowed for by the concepts used in Item No. 89034.

The part of the method of Item No. 89034 that is applicable to a plain wing with little or no sweep, where the effects of outboard flow of the boundary layer may be neglected, requires the spanwise variation of the local lift coefficient, C_{LL}, and a comparison of this with the spanwise variation of C_{Lm}, the maximum lift coefficient of the aerofoil section. For the incidence at which the peak local lift coefficient, C_{LLp} matches the local section maximum lift coefficient, C_{Lm}, the distribution of $C_{LL}c/\bar{c}$ is obtained and integrated to obtain the value of the maximum lift coefficient of the wing, C_{Lmax}. This concept is extended here to apply to a wing with a full-span trailing-edge flap and therefore the increment in C_{Lmax} due to the flap.

The same simplifying assumptions as those used in Item No. 89034 have been made to reduce the complex procedure outlined above to the calculation for only the most highly loaded spanwise station. The spanwise position, η_p, of the most highly loaded section for loading due to incidence and the corresponding normalised lift coefficient, μ_p, are shown in Figures 1 and 2 which are taken from Item No. 89034. These Figures are in terms of taper ratio, λ, and the spanwise centre of pressure location, $\bar{\eta}$, corresponding to the spanwise loading due to incidence, obtainable from Item No. 83040.

For wings with part-span flaps the procedure outlined above would need to account for the change in spanwise loading distribution due the deployment of the part-span flap. Item No. 74012 (Derivation 1) includes part-span effects, derived from a combination of theory and wind-tunnel data, for the increment in lift at a constant incidence. This has been found to be an adequate representation of part-span effects on ΔC_{Lmaxt} for plain and split flaps and is therefore incorporated in this Item. However, for slotted flaps the part-span effects on ΔC_{Lmaxt} are somewhat different and have been derived by correlation of data from Derivations 13, 15, 31 and 32.

The effects of wing sweep have been derived from an analysis of data from Derivations 14, 16, 19, 22, 23, 25, 26, 31 and 32 and require the use of geometrical characteristics for the section normal to the leading-edge at the spanwise location of maximum loading due to incidence (see Sketch 1.1), flap angle measured normal to the hinge-line and a sweep correlation factor, $K_{\Lambda t}$.

Equation (3.5) in Item No. 94028 and Equation (3.4) in Item Nos 94029 to 94031 give the general expression for the increment in maximum lift coefficient due the deployment of a trailing-edge flap on an aerofoil for the datum Reynolds number based on chord c of 3.5×10^6 as

$$\Delta C_{Lmt} = (c'/c)\Delta C'_{Lmt}, \tag{6.1}$$

where c' is the extended chord defined in Item Nos 94028 to 94031,

c is the basic aerofoil chord

and $\Delta C'_{Lmt}$ is the increment in the aerofoil maximum lift coefficient due to trailing-edge flap deployment, based on c' and derived from any of Item Nos 94028 to 94031 for a Reynolds number of 3.5×10^6.

The general expression for the maximum lift coefficient of a wing with a trailing-edge flap deployed is:

$$C_{Lmax} = C_{LmaxB} + \Delta C_{Lmaxt}, \tag{6.2}$$

where C_{LmaxB} is obtained from Item No. 89034 and is the maximum lift coefficient of the basic wing without high-lift devices deployed

and ΔC_{Lmaxt} is the increment in wing maximum lift coefficient due to the deployment of a trailing-edge flap.

6.2 Unswept Wings

For a wing with little or no sweep $(\Lambda_{1/4} \leq 5°)$

$$\Delta C_{Lmaxt} = K_f F_R (\Delta C_{Lmt}/\mu_p)(\Phi_o - \Phi_i), \tag{6.3}$$

where F_R allows for the effect of Reynolds number on the trailing-edge flap and, from Item Nos 94028 to 94031, is given by

$$F_R = 0.153 \log_{10} R_{cp} \tag{6.4}$$

and ΔC_{Lmt} is obtained from Equation (6.1) in which $\Delta C'_{Lmt}$ is derived from any of Item Nos 94028 to 94031 for given values of ρ_l/c, t/c, z_{cm}/c and $z_{u1.25}/c$ for the aerofoil section at the spanwise location η_p.

The part-span factors Φ_i and Φ_o are obtained from Figure 3a for plain and split flaps and from Figure 3b for slotted flaps as functions of $\eta(=\eta_i, \eta_o)$ and a planform parameter $A\tan\Lambda_{½} - 8\lambda$. The denominator μ_p in Equation (6.3) is the ratio of the peak local lift coefficient to the wing lift coefficient, C_{LLp}/C_L, for the loading due to incidence and is obtained from Figure 2 as a function of λ and $\bar{\eta}$.

The correlation factor K_f is dependent on the type of trailing-edge flap:-

K_f = 1.0 for plain and split flaps

and K_f = 1.1 for slotted flaps.

6.3 Swept Wings

For a swept wing ($\Lambda_{1/4} > 5°$) the increment in wing maximum lift coefficient due to the deployment of trailing-edge flaps is

$$\Delta C_{Lmaxt} = K_f K_{\Lambda t} \cos(\Lambda_h) F_R (\Delta C_{Lmt} / \mu_p)(\Phi_o - \Phi_i), \tag{6.5}$$

where F_R allows for the effect of Reynolds number on the flap and, for a swept wing, is given by

$$F_R = 0.153 \log_{10}(R_{cp} \cos^2 \Lambda_0) \tag{6.6}$$

and ΔC_{Lmt} is obtained from Equation (6.1), except that $\Delta C'_{Lmt}$ in that equation is derived from any of Item Nos 94028 to 94031 with the relevant section properties taken normal to the leading edge at η_p, and trailing-edge flap angles are now taken normal to the hinge line. The equations and Figures in Item Nos 94028 to 94031 are given in Table 6.1, and when using those equations and Figures the approximate substitutions listed in Table 6.2 should be made.

TABLE 6.1 Equations and Figures in Item Nos 94028 to 94031 requiring sweep modifications to parameters as listed in Table 6.2

Flap Type	*Plain*	*Split*	*Single-slotted*	*Double-slotted*	*Triple-slotted*
Item No.	94028	94029	94030	94031	94031
Equation Nos	(4.5)	(4.9)	(4.2) (4.3) (4.9)	(4.5) to (4.8) (4.19)	(4.5) to (4.8) (4.21) (4.22) (4.31)
Figure Nos	1	2	1 2 3 4	1 2 4 5 7 8 9	1 to 9

TABLE 6.2 Sweep modifications required in use of equations and Figures of Item Nos 94028 to 94031 given in Table 6.1

Replace	*With*
t/c	$(t/c)\sec\Lambda_0$
z_{cm}/c	$(z_{cm}/c)\sec\Lambda_0$
z_{lm}/c	$(z_{lm}/c)\sec\Lambda_0$
$(z_{u1.25}/c)_p$	$\zeta_p = (z_{u1.25}/c)_p\sec\Lambda_0$
ρ_l/c	$(\rho_l/c)\sec\Lambda_0$
δ_t, δ_t°	$\delta_t\sec\Lambda_h$, $\delta_t^\circ\sec\Lambda_h$
$(\delta_t^\circ + \phi_t^\circ)$	$(\delta_t^\circ + \phi_t^\circ)\sec\Lambda_h$
δ_{tj}, δ_{tj}°	$\delta_{tj}\sec\Lambda_h$, $\delta_{tj}^\circ\sec\Lambda_h$

Note that for simple-slotted or Fowler flap systems it is normally sufficiently accurate to take Λ_h to be the sweep of the flap leading edge in the deployed position or the sweep of the flap-shroud trailing edge.

The factor $K_{\Lambda t}$ in Equation (6.5) allows for the effect of wing sweep on the increment in maximum lift coefficient due to trailing-edge flap deployment, and has been determined empirically as

$$K_{\Lambda t} = \cos^{2.5}\Lambda_{¼}\,. \tag{6.7}$$

7. APPLICABILITY AND ACCURACY

7.1 Applicability

The method given in this Item for estimating the increment in maximum lift coefficient due to the deployment of trailing-edge flaps on a wing is applicable to straight-tapered wings covering wide ranges of planform parameters, see Table 7.1. The range of values of $A\tan\Lambda_0$ up to 8.4 encompasses rectangular wings down to A = 3 and swept wings up to A = 8 with $\Lambda_0 = 46°$. In fact, after the development of the Item, the method was found to work well for the extreme case of a cropped delta wing (A = 2.14, $\Lambda_0 = 53°$, $\lambda = 0.14$) fitted with a plain flap. Note that the forward-swept trailing edges ($\Lambda_1 < 0$) and hinge lines ($\Lambda_h < 0$) given in Table 7.1 were only associated with an unswept half-chord line ($\Lambda_{½} = 0$).

All wings used in the derivation of the Item had either a smooth surface or a narrow band of roughness near the leading edge with height just sufficient to ensure boundary-layer transition across the band.

The data used in developing the method for slotted flaps relate to flaps with a well designed slot and optimum, or near optimum, location in terms of lap and gap with respect to the wing at each flap deflection. Relatively small changes in lap and gap can have quite significant effects on the value of ΔC_{Lmaxt} achieved; the scatter in the predicted values probably reflects this to some extent (see Section 7.2). It should be noted that because of three-dimensional effects an optimum geometry determined on the basis of aerofoil/flap tests will almost certainly not be optimum when used on a wing, although it would be expected to provide a reasonable starting point. In practice, the design of a slotted flap system, aided by wind-tunnel tests, has to be something of a compromise; for example, if it is designed to be optimum (in terms of maximising ΔC_{Lmaxt} for given flow conditions, see Reference 34) at a given flap deflection, the geometry is then non-optimum at other flap deflections. Reference 33 discusses the role of the slot and its qualitative effects on the aerodynamics of the system and Derivation 20, for example, provides an experimental indication of the effects of varying slot size.

Flap support brackets used in wind-tunnel tests can give rise to problems with separation if they are not well designed and reasonably representative of the full-scale design. The method of this Item assumes that any support brackets do not have a significant effect on flap lift.

For wings with cranked leading or trailing edges or curved tips it is suggested that the calculation of the increment in maximum lift coefficient due to flap deflection be made for the equivalent straight-tapered planform as defined in Item No. 76003 (Derivation 2).

Ranges of wing and flap geometry and flow parameters used to establish the method are given in Table 7.1.

TABLE 7.1

Parameter	*Range*		
A	3	to	9
λ	0.2	to	1.0
Λ_0	0	to	50°
Λ_1	–12°	to	43°
Λ_h	–8°	to	43°
$A\tan\Lambda_0$	0	to	8.4
η_i	0	to	0.8
η_o	0.2	to	1.0
$R_{\bar{c}}\times 10^6$	0.6	to	9
M	≤ 0.25		

7.2 Accuracy

7.2.1 Unswept wings

Sketch 7.1 shows the comparison between experimental and predicted values of the increment in maximum lift coefficient due to flap deployment for split flaps, plain flaps, single-slotted flaps and double-slotted flaps on unswept wings. The experimental data were obtained from Derivations 12, 13, 15, 17, 18, 20, 21 and 30 for wings with $\Lambda_{1/4} \leq 6.4°$. Sketch 7.2 shows the comparison between experimental and predicted values of maximum lift coefficient for unswept wings with flaps deployed. In those comparisons the method of Item No. 89034 was used to predict the maximum lift coefficient for the plain wing.

For unswept wings, Sketch 7.1 shows that ΔC_{Lmaxt} is predicted to within ±10% for 90% of the data, whilst from Sketch 7.2 C_{Lmax} is predicted to within ±5 % for 88% of the data.

7.2.2 Swept wings

Sketch 7.3 shows the comparison between experimental and predicted values of the increment in maximum lift coefficient due to flap deployment for split flaps, plain flaps, single-slotted flaps and double-slotted flaps on swept wings. The experimental data were obtained from Derivations 14, 16, 19, 22, 23, 25, 26, 31 and 32. Sketch 7.4 shows the comparison between experimental and predicted values of maximum lift coefficient for swept wings with flaps deployed. In those comparisons the method of Item No. 89034 was used to predict the maximum lift coefficient for the plain wing.

For swept wings, Sketch 7.3 shows that ΔC_{Lmaxt} is predicted to within ±10% for 70% of the data, whilst Sketch 7.4 shows that C_{Lmax} is predicted to within ±5 % for 89% of the data.

Flap Type	*Part Span*	*Full Span*	*Derivation*
Plain	○	●	21
Split	□	■	12, 15, 18
Single-slotted	◇	♦	13, 15, 17, 20, 30
Double-slotted	☆	★	15

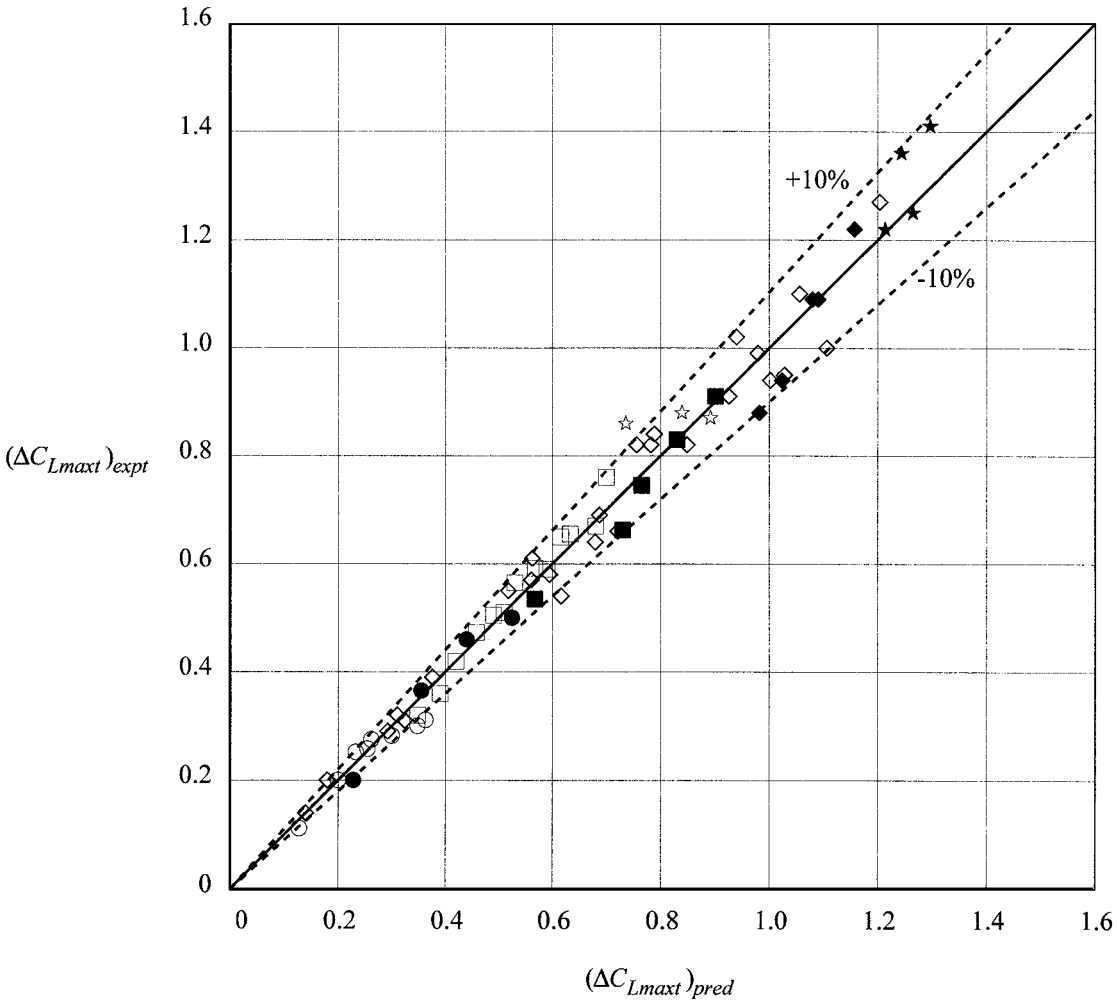

Sketch 7.1 Correlation of ΔC_{Lmaxt} for unswept wings

Flap Type	*Part Span*	*Full Span*	*Derivation*
Plain	○	●	21
Split	□	■	12, 15, 18
Single-slotted	◇	♦	13, 15, 17, 20, 30
Double-slotted	☆	★	15

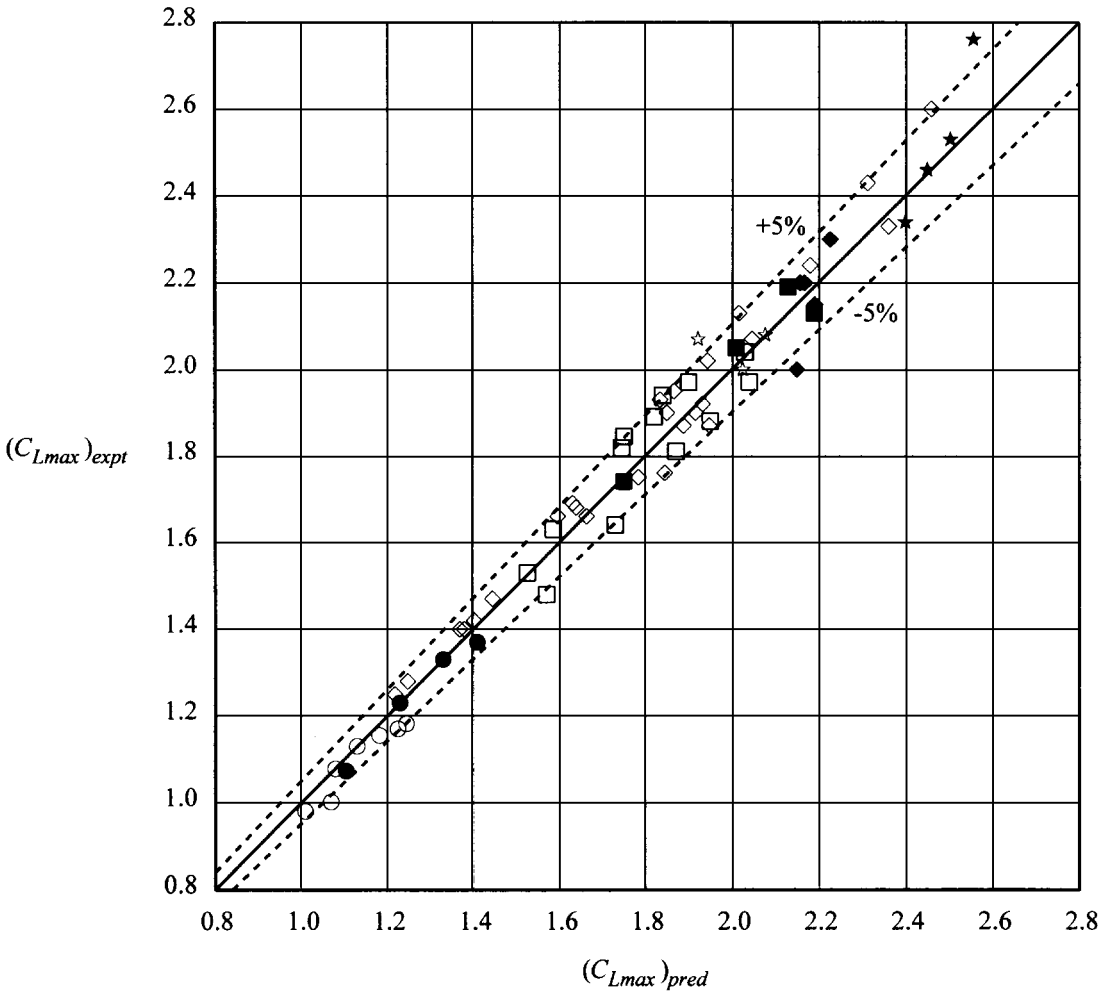

Sketch 7.2 Correlation of C_{Lmax} for unswept wing

Flap Type	*Part Span*	*Full Span*	*Derivation*
Plain	○	●	25, 32
Split	□		14, 16, 23
Single-slotted	◇	♦	19, 31
Double-slotted	☆		22, 26

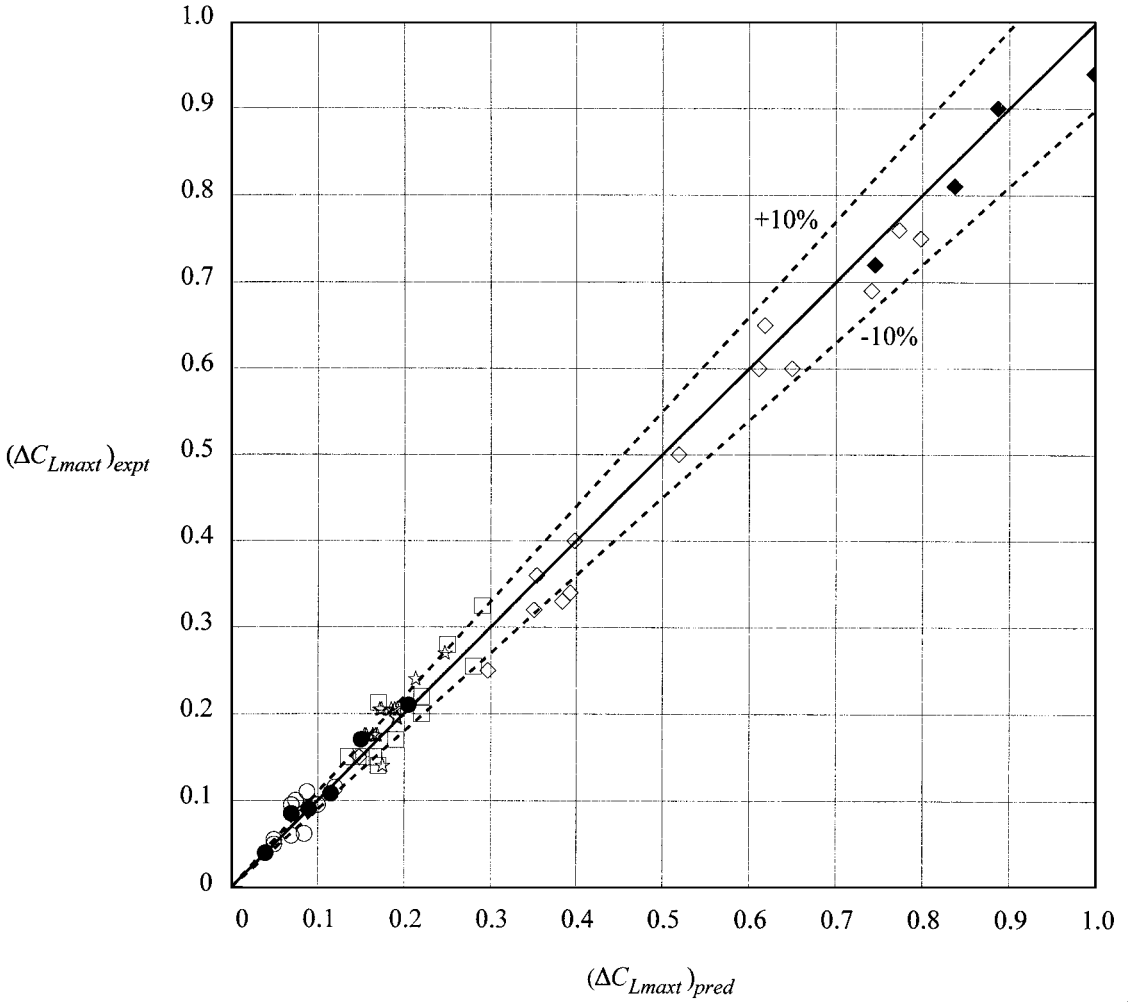

Sketch 7.3 Correlation of ΔC_{Lmaxt} for swept wings

Flap Type	*Part Span*	*Full Span*	*Derivation*
Plain	○	•	25, 32
Split	□		14, 16, 23
Single-slotted	◇	♦	19, 31
Double-slotted	☆		22, 26

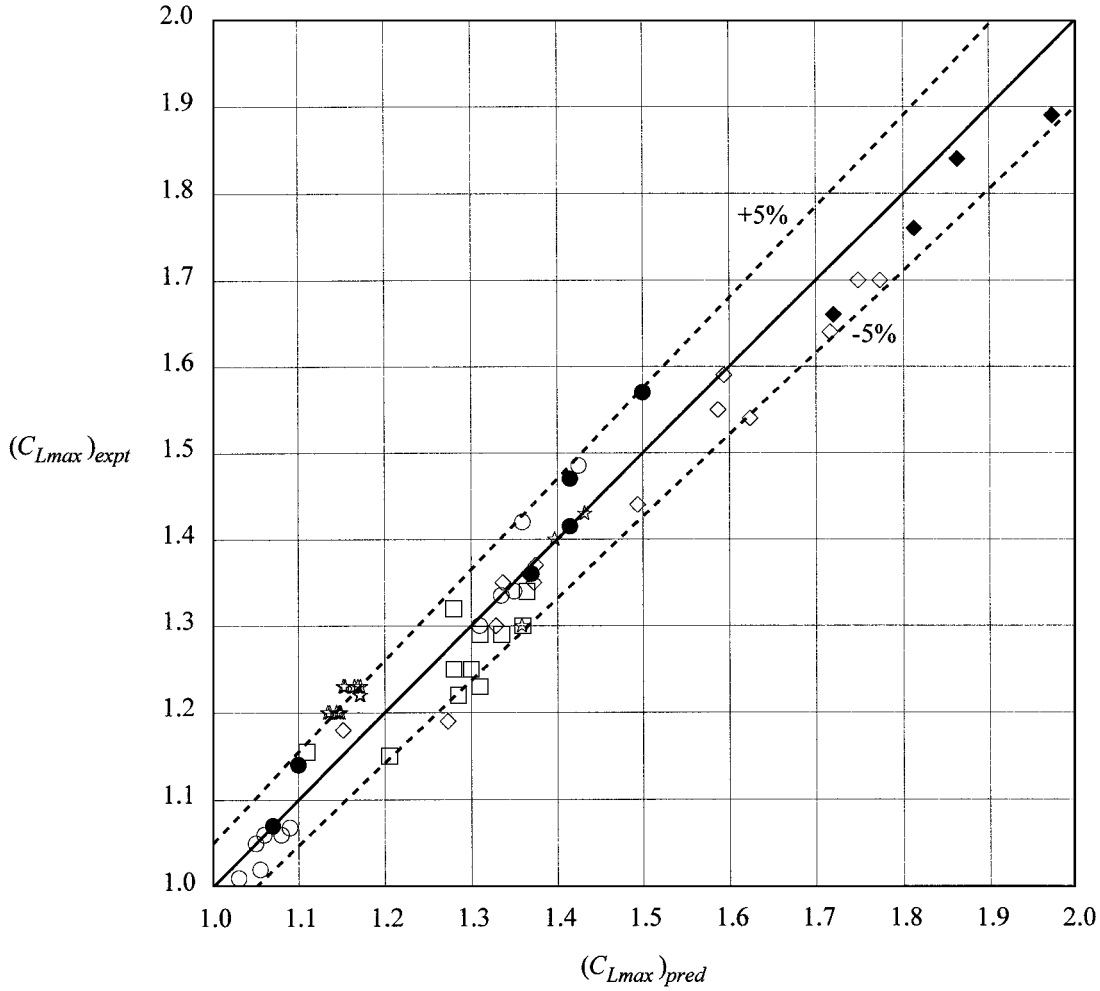

Sketch 7.4 Correlation of C_{Lmax} for swept wings

8. DERIVATION AND REFERENCES

8.1 Derivation

The Derivation lists selected sources of information that have assisted in the preparation of this Item.

8.1.1 ESDU Data Items

1. ESDU — Conversion of lift coefficient increment due to flaps from full span to part span.
ESDU International, Item No. 74012, 1974.

2. ESDU — Geometric properties of cranked and straight tapered wing planforms.
ESDU International, Item No. 76003, 1976.

3. ESDU — Method for the rapid estimation of spanwise loading of wings with camber and twist in subsonic attached flow.
ESDU International, Item No. 83040, 1983.

4. ESDU — Aerofoil maximum lift coefficient for Mach numbers up to 0.4.
ESDU International, Item No. 84026, 1984.

5. ESDU — The maximum lift coefficient of plain wings at subsonic speeds.
ESDU International, Item No. 89034, 1989.

6. ESDU — Introduction to the estimation of the lift coefficients at zero angle of attack and at maximum lift for aerofoils with high-lift devices at low speeds.
ESDU International, Item No. 94026, 1994.

7. ESDU — Increments in aerofoil lift coefficient at zero angle of attack and in maximum lift coefficient due to deployment of various leading-edge high-lift devices at low speeds.
ESDU International, Item No. 94027, 1994.

8. ESDU — Increments in aerofoil lift coefficient at zero angle of attack in maximum lift coefficient due to deployment of a plain trailing-edge flap, with or without a leading-edge high-lift device, at low speeds.
ESDU International, Item No. 94028, 1994.

9. ESDU — Increments in aerofoil lift coefficient at zero angle of attack and in maximum lift coefficient due to deployment of a trailing-edge split flap, with or without a leading-edge high-lift device, at low speeds.
ESDU International, Item No. 94029, 1994.

10. ESDU — Increments in aerofoil lift coefficient at zero angle of attack and in maximum lift coefficient due to deployment of a single-slotted trailing-edge flap, with or without a leading-edge high-lift device, at low speeds.
ESDU International, Item No. 94030, 1995.

11. ESDU — Increments in aerofoil lift coefficient at zero angle of attack and in maximum lift coefficient due to deployment of a double-slotted or triple-slotted trailing-edge flap, with or without a leading-edge high-lift device, at low speeds.
ESDU International, Item No. 94031, 1995.

8.1.2 Wind-tunnel test reports

12. WENZINGER, C.J. — Wind-tunnel investigation of tapered wings with ordinary ailerons and partial span split flaps. NACA Rep. 611, 1937.

13. HOUSE, R.O. — The effects of partial span slotted flaps on the aerodynamic characteristics of a rectangular and a tapered NACA 23012 wing. NACA tech. Note 719, 1939.

14. CONNER, D.W. NEELY, R.H. — Effects of a fuselage and various stall control flaps on aerodynamic characteristics in pitch of a NACA 64-series 40° swept-back wing. NACA RM L6L27 (TIL 1375), 1947.

15. SIVELLS, J.C. SPOONER, S.H. — Investigation in the Langley 19 foot pressure tunnel of two wings of NACA 65-210 and 64-210 airfoil sections with various type flaps. NACA Rep. 942, 1947.

16. GRAHAM, R.R. CONNER, D.W. — Investigation of high lift and stall-control devices on a NACA 64-series 42° sweptback wing with and without fuselage. NACA RM L7G09 (TIL 1407), 1947.

17. FISCHEL, J. SCHNEITER, L.E. — High speed wind tunnel investigation of high lift and aileron control characteristics of a NACA 65-210 semi-span wing. NACA tech. Note 1473, 1947.

18. LANGE, R.H. MAY, R.W. — Effect of leading-edge high lift devices and split flaps on the maximum lift and lateral characteristics of a rectangular wing of aspect ratio 3.4 with circular arc airfoil sections at Reynolds numbers from 2.9×10^6 to 8.4×10^6 . NACA RM L8D30 (TIL 1971), 1948.

19. SCHNEITER, L.E. WATSON, J.M. — Wind tunnel investigation at low speeds of various plug aileron and lift flap configurations on a 42° sweptback semi-span wing. NACA RM L8K19 (TIL 2058), 1948.

20. FISCHEL, J. VOGLER, R.D. — High lift and lateral control characteristics of a NACA 65_2-215 semi-span wing equipped with plug and retractable ailerons and a full span flap. NACA tech. Note 1872, 1949.

21. JOHNSON, H.S. HAGERMAN, J.R. — Wind tunnel investigation at low speed of an unswept untapered semi-span wing of aspect ratio 3.13 equipped with various 25-per-cent-chord plain flaps. NACA tech. Note 2080, 1950.

22. SALMI, R.J — Effects of leading-edge device and trailing-edge flaps on longitudinal characteristics of two 47.7° sweptback wings of aspect ratio 5.1 and 6 at a Reynolds number of 6.0×10^6 . NACA RM L50F20 (TIL 2466), 1950.

23. PRATT, G.L. SHIELDS, R.R. — Low speed longitudinal characteristics of a 45° sweptback wing of aspect ratio 8 with high lift and stall control devices at Reynolds numbers from 1,500,000 to 4,800,000. NACA RM L51J04 (TIL 3038), 1952.

24. YOUNG, A.D. — The aerodynamic characteristics of flaps. ARC R&M 2622, 1953.

25. WHITTLE, E.F. LIPSON, S. — Effect on the low speed aerodynamic characteristics of a 49° sweptback wing having an aspect ratio of 3.78 of blowing air over the trailing-edge flap and aileron. NACA RM L54C05 (TIL 4196), 1954.

26. NAESETH, R.L. — Low speed longitudinal aerodynamic characteristics of a 45° sweptback wing with double-slotted flaps. NACA RM L56A10 (TIL 5052), 1956.

27. ROSHKO, A. — Computation of the increment of maximum lift due to flaps. Douglas Report SM-23626, 1959.

28. McRAE, D.M. — The aerodynamics of high-lift devices on conventional aircraft. *Aeronaut. J.*, Vol. 73, pp. 535 to 541, June 1969.

29. SANDERS, K.L. — High lift devices, a weight and performance tradeoff methodology. Ryan Aeronautical Company, Technical Paper 761, 1969.

30. PAULSON, J.W. — Wind-tunnel investigation of a Fowler flap and spoiler for an advanced general aviation wing. NASA tech. Note D-8236, 1976.

31. LOVELL, D.A. — A wind-tunnel investigation of the effects of flap span and deflection angle, wing planform and body on the high lift performance of a 28° swept wing. RAE tech. Rep. 76030, 1976.

32. RAE — Unpublished data, 1978.

8.2 References

The References list sources of information supplementary to that given in this Item.

33. SMITH, A.M.O. — High-lift aerodynamics. *J. Aircr.*, Vol. 12, No. 6, pp. 501 to 530, June 1975.

34. FIDDES, S.P. KIRBY, D.A. WOODWARD, D.S. PECKHAM, D.H. — Investigations into the effects of scale and compressibility on lift and drag in the RAE 5m pressurised low-speed wind-tunnel. *Aeronaut. J.*, Vol. 89, pp. 93 to 108, March 1985.

35. ESDU — Maximum lift of wings with leading-edge devices and trailing-edge flaps deployed. ESDU International Item No. 92031, 1992.

9. EXAMPLE

Estimate the increment in maximum lift coefficient for a wing with a plain trailing-edge flap for a Reynolds number $R_{\bar{c}} = 7 \times 10^6$ and a free-stream Mach number $M = 0.2$.

The wing has planform geometry parameters

$$A = 8,\ \Lambda_{¼} = 25°\ \text{and}\ \lambda = 0.4$$

and a constant section, NACA 63_1-212, across the span for which

$$t/c = 0.12,\ \rho_l/c = 0.01087,\ \text{and}\ \phi_t^\circ = 7.7° .$$

The plain flap has streamwise section geometry

$$c_t/c = 0.3\ \text{and}\ \delta_t^\circ = 35°$$

and extends from the wing centre-line $(\eta_i = 0)$ to 60% semi-span $(\eta_0 = 0.6)$.

1. Check that the sweep angles are within the range of applicability of the method

From the relationships for planform geometry given in Item No. 76003,

$$\Lambda_0 = \tan^{-1}\left[\tan\Lambda_{¼} + \frac{1}{A}\left(\frac{1-\lambda}{1+\lambda}\right)\right]$$

$$= \tan^{-1}\left[\tan 25° + \frac{1}{8}\left(\frac{1-0.4}{1+0.4}\right)\right]$$

$$= 27.5°.$$

$$\Lambda_1 = \tan^{-1}\left[\tan\Lambda_{¼} - \frac{3}{A}\left(\frac{1-\lambda}{1+\lambda}\right)\right]$$

$$= \tan^{-1}\left[\tan 25° - \frac{3}{8}\left(\frac{1-0.4}{1+0.4}\right)\right]$$

$$= 17.0°.$$

The hinge-line sweep angle, Λ_h, is that of the 0.7 chord line, *i.e.*

$$\Lambda_h = \tan^{-1}\left[\tan\Lambda_{¼} + \frac{4}{A}\left(\frac{1}{4} - 0.70\right)\left(\frac{1-\lambda}{1+\lambda}\right)\right]$$

$$= 20.3°.$$

From Table 7.1 it is seen that the values of Λ_0, Λ_1 and Λ_h all lie within the permitted ranges.

2. Determine the required wing planform parameters

From the relationship in Item No. 76003, with the given values of A, $\Lambda_{¼}$ and λ

$$A\tan\Lambda_{½} = A\tan\Lambda_{¼} - \frac{1-\lambda}{1+\lambda}$$

$$= 8\times\tan 25° - \frac{1-0.4}{1+0.4}$$

$$= 3.302.$$

The wing taper parameter κ is given by

$$\kappa = \frac{1+2\lambda}{3(1+\lambda)}$$

$$= \frac{1+2\times 0.4}{3(1+0.4)}$$

$$= 0.429.$$

3. Determine $\bar{\eta}$ from Item No. 83040

Since $M = 0.2$,

$$\beta A = (1-M^2)^{½}A$$

$$= (1-0.2^2)^{½}\times 8$$

$$= 7.84,$$

and so with $A\tan\Lambda_{½} = 3.302$ and $\kappa = 0.429$ a cross-plot in βA using Figures 1 to 5 of Item No. 83040 gives

$$\bar{\eta} = 0.437.$$

4. Determine η_p

From Figure 1, with $\bar{\eta} = 0.437$ and $\lambda = 0.4$,

$$\eta_p = 0.69.$$

5. Determine μ_p

From Figure 2, with $\bar{\eta} = 0.437$ and $\lambda = 0.4$,

$$\mu_p = 1.15.$$

6. Determine $R_{cp}\cos^2\Lambda_0$ appropriate to η_p

For $\lambda = 0.4$, and $\eta_p = 0.69$ the streamwise chord c_p at η_p is given by

$$c_p / \bar{\bar{c}} = \frac{3}{2}\left[\frac{1+\lambda}{1+\lambda+\lambda^2}\right](1-\eta_p+\lambda\eta_p)$$

$$= \frac{3}{2}\left[\frac{1+0.4}{1+0.4+0.4^2}\right](1-0.69+0.4\times 0.69)$$

$$= 0.7888.$$

The Reynolds number at η_p is given by

$$R_{cp} = R_{\bar{\bar{c}}} \times c_p / \bar{\bar{c}}$$

$$= 7\times 10^6 \times 0.7888$$

$$= 5.522\times 10^6.$$

Hence

$$R_{cp}\cos^2\Lambda_0 = 5.522\times 10^6 \times \cos^2(27.5°)$$

$$= 4.345\times 10^6.$$

7. Determine ΔC_{Lmt} using Item No. 94028

Section 6.3 shows that the following parameters are required for use in Item No. 94028:

$$\delta_t \sec\Lambda_h = (35° \times \pi/180) \times \sec 20.3°$$

$$= 0.651 \text{ rad.}$$

and

$$(\delta°_t + \phi°_t)\sec\Lambda_h = (35° + 7.7°) \times \sec(20.3°)$$

$$= 45.53°.$$

Figure 1 of Item No. 94028, with " $\delta^\circ_t + \phi^\circ_t$ " $= (\delta^\circ_t + \phi^\circ_t)\sec\Lambda_0 = 45.53^\circ$, gives

$$J_p = 0.443 .$$

Thus, Equation (4.5) of Item No. 94028 with $J_p = 0.443$, "δ_t" $= \delta_t \sec\Lambda_h = 0.651$ rad. and $c_t/c' = c_t/c = 0.3$ (since $c' = c$ for a plain flap) gives

$$\begin{aligned}\Delta C'_{L0t} &= 2J_p\delta_t\left\{\pi - \cos^{-1}(2c_t/c' - 1) + [1-(2c_t/c'-1)^2]^{½}\right\}\\ &= 2\times 0.443\times 0.651\times\left\{\pi - \cos^{-1}(2\times 0.3 - 1) + [1-(2\times 0.3-1)^2]^{½}\right\}\\ &= 1.197.\end{aligned}$$

Now*, for $\rho_l/t = (\rho_l/c)/(t/c) = 0.01087/0.12 = 0.0906$, Equation (4.9) of Item No. 94028 gives

$$\begin{aligned}K_G &= 1.225 + 4.525\rho_l/t\\ &= 1.225 + 4.525 \times 0.0906\\ &= 1.635.\end{aligned}$$

Equation (4.10) of Item No. 94028 gives

$$K_t = 0.8$$

and Figure 2 of Item No. 94028 with $x_s/c' = 0$ and $c_t/c' = 0.3$, gives

$$T = 0.442,$$

so that Equation (4.8) of Item No. 94028 gives

$$\begin{aligned}\Delta C'_{Lmt} &= K_G K_t T \Delta C'_{L0t}\\ &= 1.635 \times 0.8 \times 0.442 \times 1.197\\ &= 0.692.\end{aligned}$$

Therefore, for the aerofoil/flap combination normal to the leading edge at $\eta = \eta_p$, Equation (6.1) gives

$$\begin{aligned}\Delta C_{Lmt} &= (c'/c)\Delta C'_{Lmt}\\ &= 1.0 \times 0.692\\ &= 0.692.\end{aligned}$$

* In theory both ρ_l/c and t/c should be factored by sec Λ_0 but when ρ_l/t is formed the factors cancel and are omitted here.

8. Determine Φ_o and Φ_i

Figure 3a, for $A\tan\Lambda_{½} - 8\lambda = 3.302 - 8\times 0.4 = 0.102$ and $\eta_o = 0.6$ gives

$$\Phi_o = 0.755$$

and for $\eta_i = 0$

$$\Phi_i = 0\,.$$

9. Determine ΔC_{Lmaxt}

Equation (6.5) gives

$$\Delta C_{Lmaxt} = K_f K_{\Lambda t}\cos(\Lambda_h) F_R(\Delta C_{Lmt}/\mu_p)(\Phi_o - \Phi_i)$$

where, from Equation (6.6),

$$\begin{aligned} F_R &= 0.153\log_{10}(R_{cp}\cos^2\Lambda_0) \\ &= 0.153\times\log_{10}(4.345\times 10^6) \\ &= 1.0156, \end{aligned}$$

and, from Equation (6.7),

$$\begin{aligned} K_{\Lambda t} &= \cos^{2.5}\Lambda_{¼} \\ &= \cos^{2.5}25° \\ &= 0.782. \end{aligned}$$

From Section 6.2, $K_f = 1.0$ for a plain flap.

Thus,

$$\begin{aligned} \Delta C_{Lmaxt} &= 1.0\times 0.782\times\cos 20.3°\times 1.0156\times(0.692/1.15)\times(0.755-0) \\ &= 0.338. \end{aligned}$$

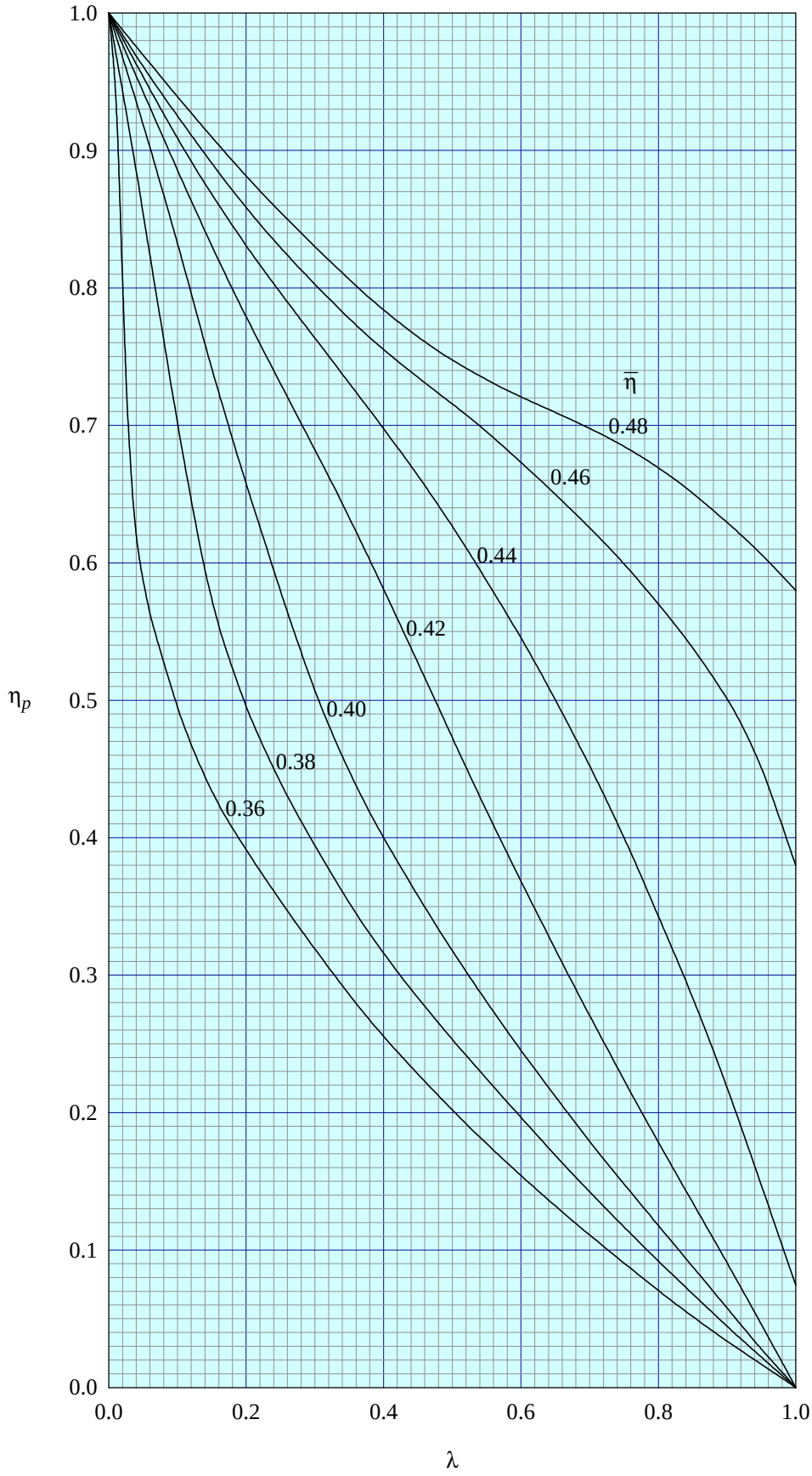

FIGURE 1 VARIATION OF η_p WITH λ AND $\bar{\eta}$

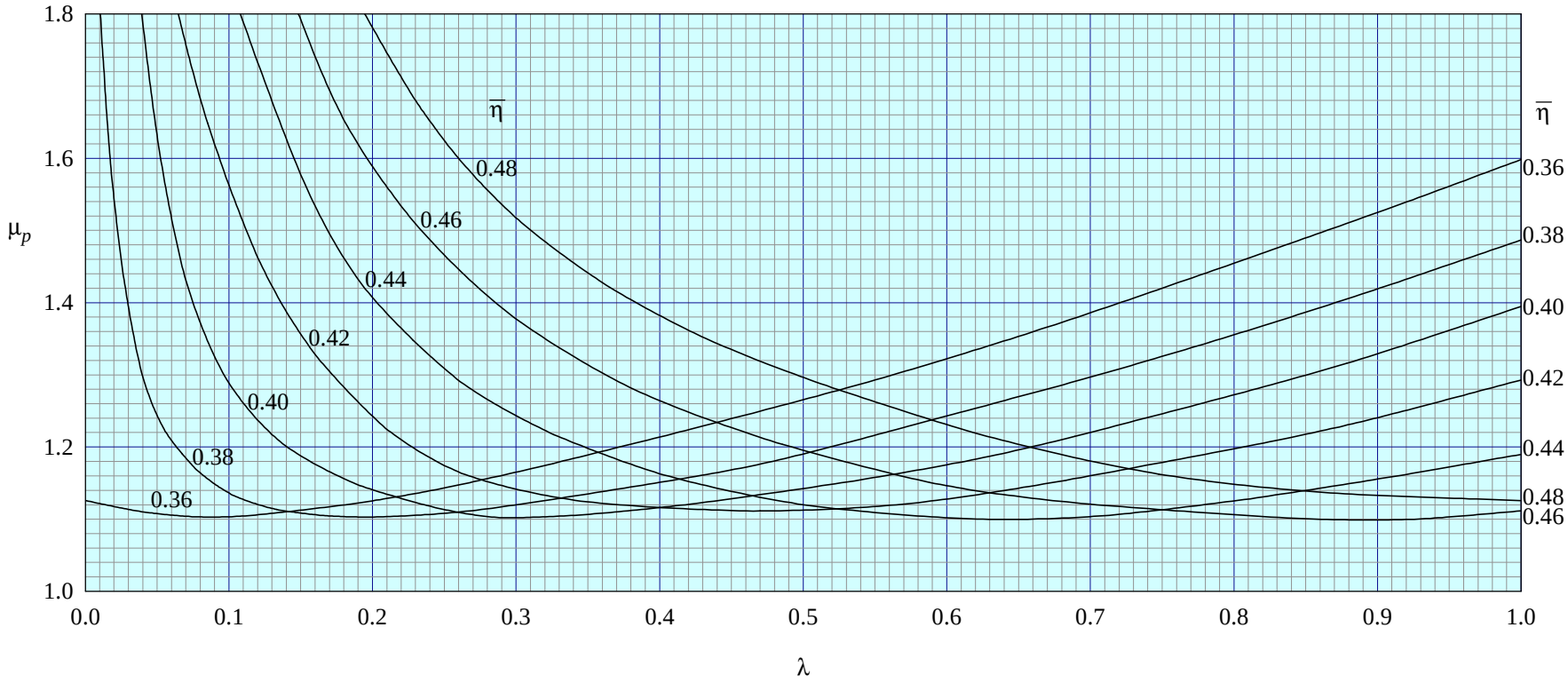

FIGURE 2 VARIATION OF μ_p WITH λ AND $\bar{\eta}$

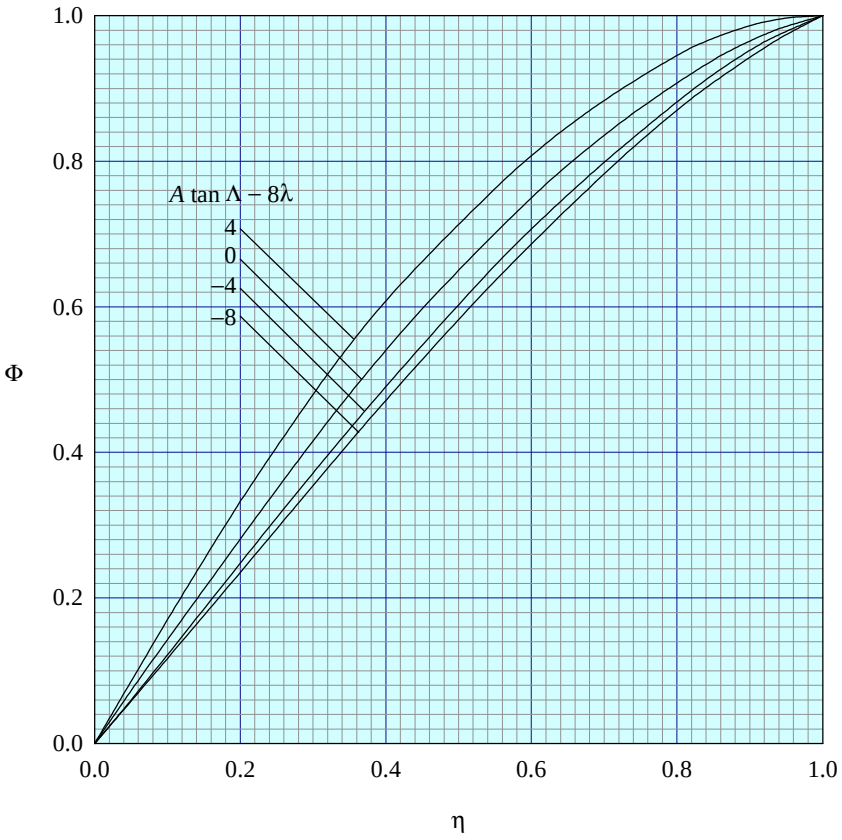

FIGURE 3a PART-SPAN FACTOR FOR PLAIN AND SPLIT FLAPS

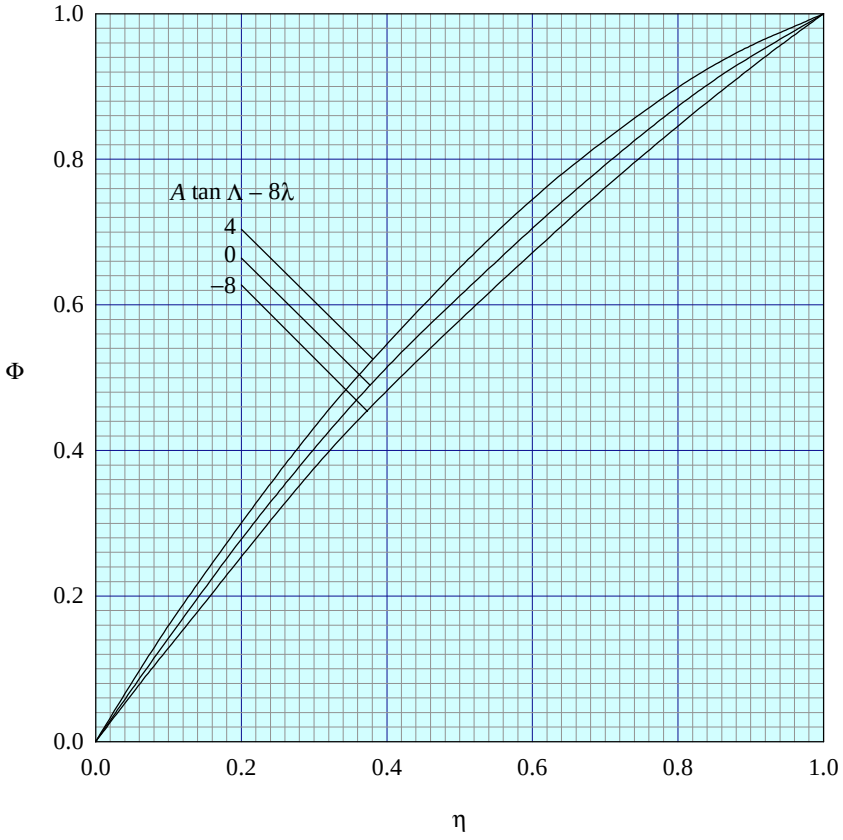

FIGURE 3b PART-SPAN FACTOR FOR SLOTTED FLAPS

THE PREPARATION OF THIS DATA ITEM

The work on this particular Item was monitored and guided by the Aerodynamics Committee which first met in 1942 and now has the following membership:

Chairman

Mr H.C. Garner – Independent

Members

Mr G.E. Bean*	–	Boeing Commercial Airplane Co., Seattle, Wash., USA
Dr N.T. Birch	–	Rolls-Royce plc, Derby
Dr P.C. Dexter	–	British Aerospace plc, Sowerby Research Centre, Bristol
Mr J.R.J. Dovey	–	Independent
Dr K.P. Garry	–	Cranfield University
Mr D. Graham*	–	Northrop Grumman Corp., Pico Rivera, Calif., USA
Mr M.J. Green	–	Avro International Aerospace Ltd, Woodford
Dr H.P. Horton	–	Queen Mary and Westfield College, University of London
Dr D.W. Hurst	–	University of Southampton
Mr P.K. Jones	–	Independent
Mr K. Karling*	–	Saab-Scania AB, Linköping, Sweden
Mr M. Maurel	–	Aérospatiale, Toulouse, France
Mr C.M. Newbold	–	Aircraft Research Association, Bedford
Mr J.B. Newton	–	British Aerospace Defence Ltd, Warton
Mr R. Sanderson	–	Daimler-Benz Aerospace Airbus GmbH, Bremen, Germany
Mr A.E. Sewell*	–	McDonnell Douglas Corp., Long Beach, Calif., USA
Mr M.R. Smith	–	British Aerospace Airbus Ltd, Bristol
Mr J. Tweedie	–	Short Brothers plc, Belfast.

* Corresponding Member

The technical work in the assessment of the available information and the construction and subsequent development of the Data Item was carried out under contract to ESDU by Mr J.R.J. Dovey.